Geochemical Perspectives Letters

Ikaite precipitation indicates near surface occurrence of methane in an Icelandic fjord

A. Hylén[1,2*], S. Arndt[3,4], J.P. Balmonte[5], R. Bosman[6], W. Bui[3], L. Chou[3], I. Delbono[7], C. Goossens[1], P.O.J. Hall[8], S. Hidalgo-Martinez[1], R.K. James[3,9], M. Kononets[8,10], P. Ley[1], C. März[11], S.P. Purayil[12], J. Reardon[13], P. Reyniers[14], F. Sales de Freitas[3], L. Verweirder[14], K. Wagner[11], C. Wittig[15], K.R. Hendry[16,17], S.J. van de Velde[1,18,19]

OPEN ACCESS

https://doi.org/10.7185/geochemlet.2621

Abstract

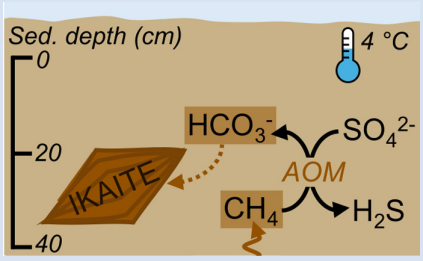

Climate change driven release of methane (CH_4) from polar and sub-polar sediments could accelerate global warming, and tracking CH_4 in cold sediments over geological time helps predict future releases. Isotopic signatures of ikaite ($CaCO_3{\cdot}6H_2O$) and its pseudomorph, glendonite, may be used to identify past CH_4 in cold environments, as alkalinity (A_T) from anaerobic oxidation of methane (AOM) can induce precipitation of this mineral at low temperatures. However, the suitability of ikaite as a proxy for CH_4 near the sediment surface remains uncertain, as ikaite linked to modern seeps has only been retrieved from sediment depths of several metres. We report ikaite crystals in surface sediments (0–40 cm depth) in Reyðarfjörður, Iceland. High A_T fluxes from deeper sediment layers and low stable carbon isotope ($\delta^{13}C$) values of the ikaite (–49.8 to –53.8 ‰) suggest formation from AOM, while sub-bottom profiling indicates shallow gas below the sampling site. As such, the recovered ikaite provides indirect evidence that CH_4 locally reaches shallow sediment layers in the studied fjord, considerably expanding the environmental range of CH_4-derived ikaite and substantiating ikaite and glendonite as proxies for cold environment CH_4 seeps.

Received 14 January 2026 | Accepted 5 May 2026 | Published 18 June 2026

Introduction

The large reservoirs of methane (CH_4) in Arctic and sub-Arctic marine sediments are of considerable interest due to their potential destabilisation from global warming (James *et al.*, 2016). Identifying CH_4 reservoirs is crucial for understanding their stability, as is tracking their occurrences and responses to climate change over geological time. Since the anaerobic oxidation of methane (AOM) produces alkalinity (A_T) and can induce authigenic carbonate precipitation in sediments, carbonates can be used to trace CH_4 reservoirs by their stable carbon isotope ($\delta^{13}C$) composition (Campbell, 2006; Vickers *et al.*, 2022).

1. Geobiology Research Group, Department of Biology, University of Antwerp, Universiteitsplein 1, 2610 Wilrijk, Belgium
2. Aix-Marseille Université, CNRS, IRD, INRAE, CEREGE, Technopôle de l'Arbois-Méditerranée, BP80, 13545 Aix-en-Provence, France
3. BGeoSys, Department of Geosciences, Society and Environment, Université Libre de Bruxelles, CP160/02, 50 Avenue F.D. Roosevelt, 1050 Brussels, Belgium
4. iC3, Department of Geoscience, Arctic University of Norway, Tromsø, Norway
5. Department of Earth and Environmental Sciences, Lehigh University, USA
6. Institute for Biochemistry and Signal Transduction, University Medical Center Hamburg-Eppendorf, Martinistraße 52, 20246 Hamburg, Germany
7. ENEA Marine Environment Research Centre, Department for Sustainability, Laboratory of Biodiversity and Ecosystems, 19032 Pozzuolo di Lerici (La Spezia), Italy
8. Department of Marine Sciences, University of Gothenburg, Box 461, 405 30 Gothenburg, Sweden
9. Department of Biology, University of Southern Denmark, Odense Denmark
10. Research consultant, Fredrikas Gård 2, 414 83, Gothenburg, Sweden
11. Institute for Geosciences, University of Bonn, Kirschallee 1-3, 53115 Bonn, Germany
12. Operational Directorate Natural Environment, Royal Belgian Institute of Natural Sciences, Brussels, Belgium
13. External Relations Team, University of Southern Denmark, Odense, Denmark
14. Department of Geology, Ghent University, Krijgslaan 297, 9000 Ghent, Belgium
15. Marine Biology Research Group, Ghent University, Ghent, Belgium
16. British Antarctic Survey, High Cross, Madingley Road, Cambridge, CB3 0ET, UK
17. Queens' College, University of Cambridge, Silver Street, Cambridge, CB3 9ET, UK
18. Department of Marine Science, University of Otago, Ōtepoti Dunedin, 9016, Aotearoa New Zealand
19. Earth Sciences New Zealand, Te Whanganui-a-Tara Wellington, 6021, Aotearoa New Zealand

* Corresponding author (email: hylen@cerege.fr)

Isotopically heavy carbonates (> −5 ‰) indicate incorporation of residual dissolved inorganic carbon (DIC) from methanogenesis, while isotopically light carbonates (< −30 ‰) precipitate from DIC formed through AOM. By contrast, carbonates formed from DIC released during organic matter mineralisation have $\delta^{13}C$ values around −25 ‰.

The mineral ikaite ($CaCO_3{\cdot}6H_2O$) (Pauly, 1963) is of particular interest as an indicator of CH_4 and AOM. It forms at low temperatures (<6 °C) under highly alkaline conditions, where inhibitors such as phosphate and organic compounds suppress the precipitation of less soluble calcium carbonate phases, such as calcite and aragonite (Lu *et al.*, 2012; Zhou *et al.*, 2015; Tollefsen *et al.*, 2018). Because of this temperature dependence, ikaite and its pseudomorph glendonite are used as proxies for cold conditions in palaeoenvironmental reconstructions (Rogov *et al.*, 2021; Schultz *et al.*, 2022; Vickers *et al.*, 2022), and their $\delta^{13}C$ signatures and presence have been applied to identify modern and past CH_4 seeps in cold systems (Schubert *et al.*, 1997; Greinert and Derkachev, 2004; Teichert and Luppold, 2013; Morales *et al.*, 2017).

Although ikaite suggested to have formed due to intense organic matter degradation has been found near the sediment surface (Kennedy, 2022), ikaite linked with CH_4 and AOM has only been retrieved from 1–4 m sediment depth (Schubert *et al.*, 1997; Lu *et al.*, 2012; Hiruta and Matsumoto, 2022; Kolesnik *et al.*, 2025; also see references in Schultz *et al.*, 2022). How well ikaite and glendonite trace CH_4 occurrences at the sediment-water interface thus remains unclear. Here, we report the occurrence of ikaite crystals in the surface sediment (top 40 cm) of Reyðarfjörður, Iceland. Sediment geochemistry and low ikaite $\delta^{13}C$ values indicate that the mineral formed as a result of AOM. This observation substantially extends the known depth range of CH_4 derived ikaite (Teichert and Luppold, 2013; Morales *et al.*, 2017), supporting its use for tracing past occurrences of CH_4 at the sediment surface, and demonstrates, for the first time, the presence of ikaite in Icelandic waters (Rogov *et al.*, 2021).

Site Description and Sampling

Samples were collected in Reyðarfjörður (Fig. 1a), eastern Iceland, aboard the R/V *Belgica* on July 8, 2023. Sampling and analytical methods are detailed in the Supplementary Information. The fjord is not influenced by active volcanic systems (Thordarson and Höskuldsson, 2008). The sampling site RF2 (65° 0.9021′ N; 13° 53.5279′ W; 150 m depth) is located

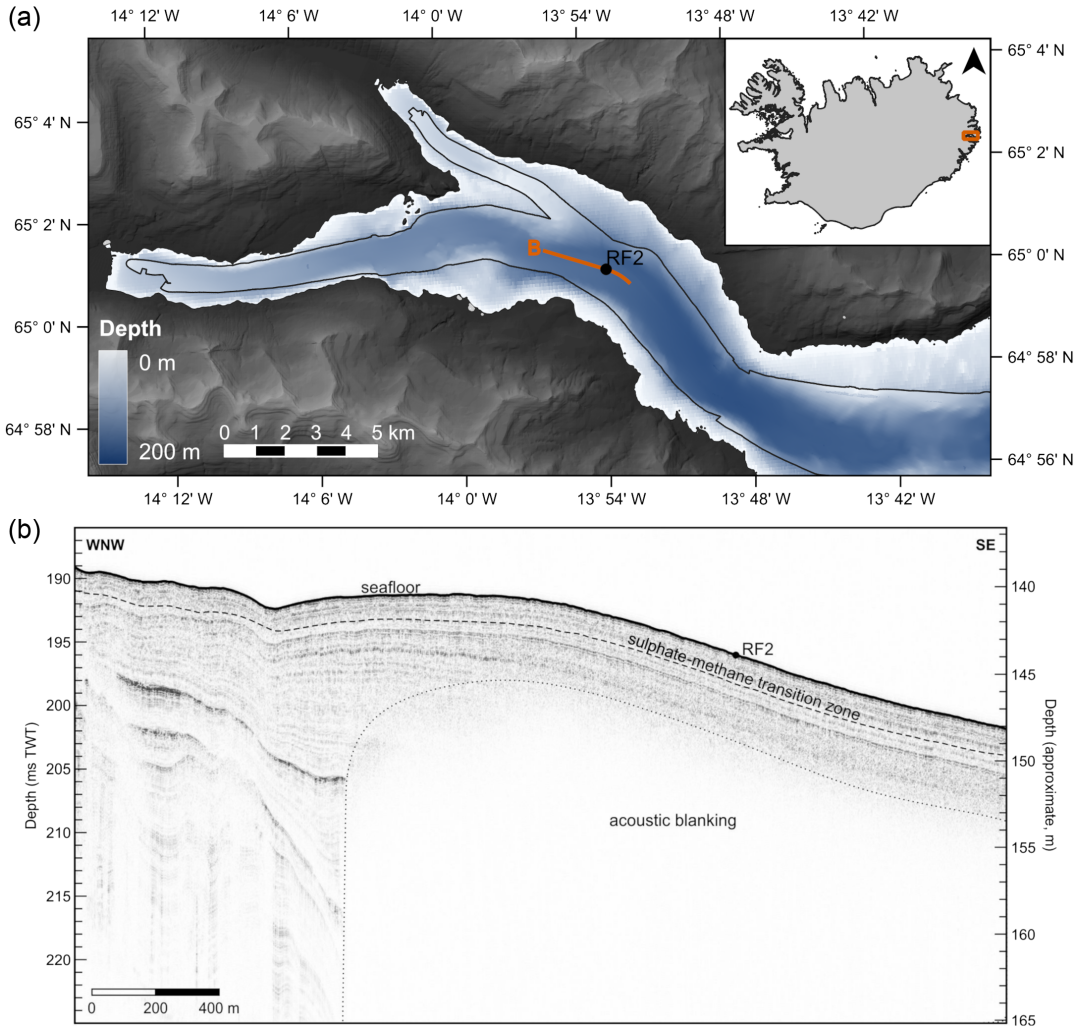

Figure 1 **(a)** Map of the sampling site (RF2) in Reyðarfjörður, eastern Iceland. The area within the black line shows the bottom topography as mapped by multibeam echo sounder. The orange line shows the location of the sub-bottom transect in panel B. The map was produced with the datasets LMI Digital Elevation Model, IS 50V Strandlína and IS 50V Vatnafar from Náttúrufræðistofnun, licensed under CC BY 4.0, and the EMODnet Bathymetry Consortium (2024). **(b)** Sub-bottom transect showing acoustic blanking below station RF2, suggesting the presence of gas. TWT = two way travel time.

above an area of acoustic blanking identified by a hull mounted TOPAS profiler (Fig. 1b), indicating sub-seafloor gas (Judd and Hovland, 1992). Prior to sediment sampling, CTD measurements 5 m above the seafloor recorded a salinity of 34.4, a temperature of 4.2 °C, and a dissolved oxygen (O_2) concentration of 287 µmol kg^{-1}.

Sediment for geochemical profiling was collected using a GEMAX corer (Ø 9 cm). One set of cores was used for microsensor profiling for O_2, hydrogen sulphide (H_2S), and pH. Replicate cores were sliced and centrifuged to separate solids from porewater. The solid phase was analysed for particulate organic and inorganic carbon (POC, PIC), their stable isotope compositions ($\delta^{13}C_{POC}$, $\delta^{13}C_{PIC}$), mineralogy, and the contents of iron oxides, acid volatile sulphide (AVS), and chromium reducible sulphide (CRS). Porewater was analysed for DIC, total alkalinity (A_T), dissolved phosphorus, sulphur, calcium, and magnesium. Porewater concentrations of DIC and A_T were used to calculate pH and the saturation states of calcite and aragonite. An additional sediment core was collected for ^{210}Pb and ^{137}Cs dating.

A box corer (Ø 50 cm) was used to collect the upper 40 cm of sediment for flux incubations. Three replicate cores, collected 5 m apart, were sub-cored into incubation chambers (Ø 14.4 cm; Fig. S-1) for measuring sediment-water fluxes of DIC (including $\delta^{13}C$ composition; $\delta^{13}C_{DIC}$), A_T, and O_2. The top 5 cm of all cores were brown and bioturbated, but deeper layers varied: two were grey to dark grey, and one was black. Owing to these visual differences, the black core was designated RF2I. Repeated attempts to relocate RF2I-type sediment were unsuccessful, indicating strong local heterogeneity.

Multiple crystals resembling ikaite (Fig. 2a) were found at 20–40 cm sediment depth at RF2I. One crystal was analysed by single crystal XRD under a nitrogen gas cryostream, and the stable isotope composition ($\delta^{13}C_{ikaite}$ and $\delta^{18}O_{ikaite}$) was measured at two points on another (Fig. 2b). Following the flux incubation, the RF2I sediment was sub-cored (Ø 5.9 cm) to <20 cm sediment depth for solid phase carbon and mineralogy analyses, microprofiles of O_2, pH and H_2S, and measurement of porewater DIC and A_T. No ikaite crystals were found in the incubated sediment.

Sediment Geochemistry

The sediment geochemistry reflected the visual differences between RF2 and RF2I (Fig. S-1). At RF2, porewater A_T and DIC increased from 2.6 mmol kg^{-1} at the surface to 7.0 mmol kg^{-1} at depth, with O_2 penetrating 0.4 cm (Fig. 3). In contrast, the RF2I sediment was heterogeneous and showed signs of more intense diagenesis. In one replicate core, the porewater A_T and DIC increased from 3.0 mmol kg^{-1} at the surface to 15 mmol kg^{-1} at depth, while in a second core, they reached 20–25 mmol kg^{-1}, with A_T clearly exceeding DIC. The O_2 penetration depths clustered into two groups at 0.1 and 0.3 cm, and a strong H_2S odour was present. At both sites, measured and calculated porewater pH profiles were in agreement. The calculated pH is sensitive to small DIC and A_T losses during sampling, so profiles should be seen as general trends. At both sites, pH decreased in the upper centimetres, stabilising near 7.5 at RF2 but increasing with depth to ~9 at RF2I, particularly in the core with high A_t and DIC.

The geochemical differences between RF2 and RF2I were not due to variations in organic matter degradation, as POC contents were similar (Fig. 3). No differences in mineralogy as determined by powder XRD were observed between sites (Fig. S-2). Instead, linear increases in the DIC and A_T at the bottom of the porewater profiles suggest upward diffusion from deeper sediment layers at both locations, with considerably steeper concentration gradients indicating stronger upward fluxes at RF2I.

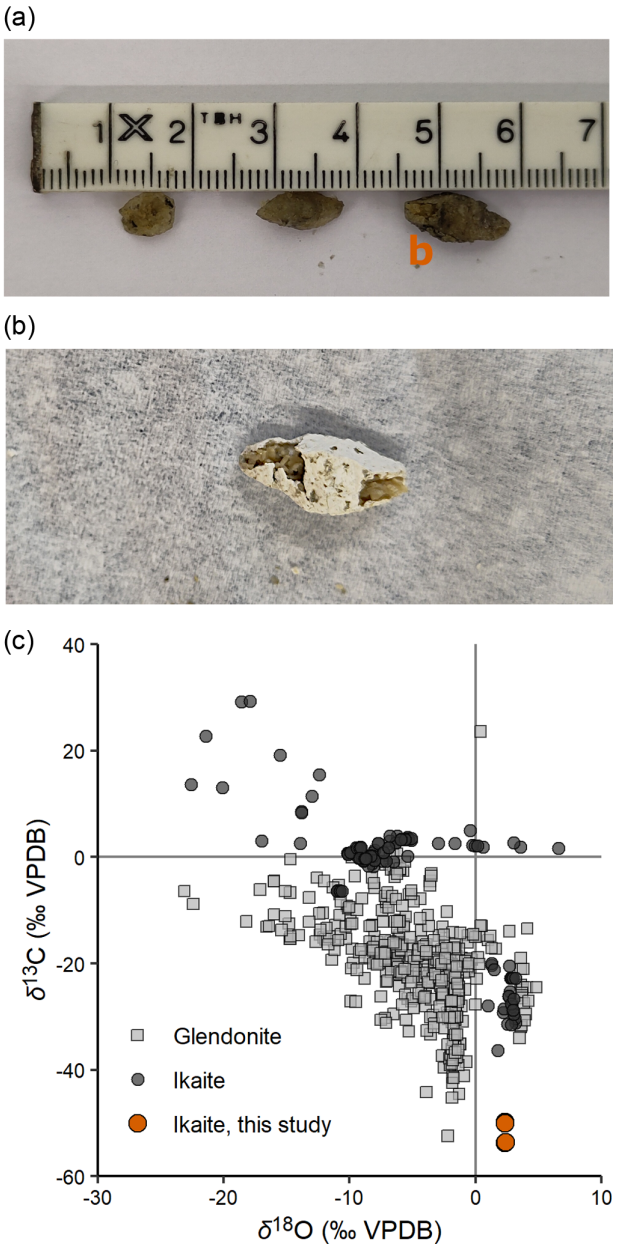

Figure 2 **(a)** Photograph of three of the ikaite crystals found at RF2I. **(b)** Photograph of a dried, recrystallised ikaite crystal marked with 'b' in panel **(a)**. **(c)** Global compilation of isotopic compositions of glendonite and ikaite (Rogov *et al.*, 2021), including the ikaite from this study.

Elevated pH, and DIC and A_T concentrations are consistent with AOM (Campbell, 2006) and suggest a deep CH_4 source, plausibly connected to the area of acoustic blanking seen in the TOPAS profile (Fig. 1b). Although AOM typically produces H_2S *via* sulphate reduction (Egger *et al.*, 2018) and a strong H_2S odour was noted during coring, no H_2S was detected in the top 4 cm of sediment. This absence of H_2S is consistent with high ferric iron contents (200–300 µmol g^{-1}) at 2–15 cm depth at station RF2, which could scavenge H_2S as iron sulphides (AVS and CRS; Fig. S-3; Berner, 1970).

Despite contrasting porewater profiles at RF2 and RF2I, the measured sediment-water fluxes of A_T, DIC, and O_2 were similar across both sites (Fig. 4a). Interestingly, diffusive O_2 uptake rates calculated from microprofiles at RF2I clustered into two groups at 16–20 mmol m^{-2} d^{-1} and 5–6 mmol m^{-2} d^{-1}, whereas the total O_2

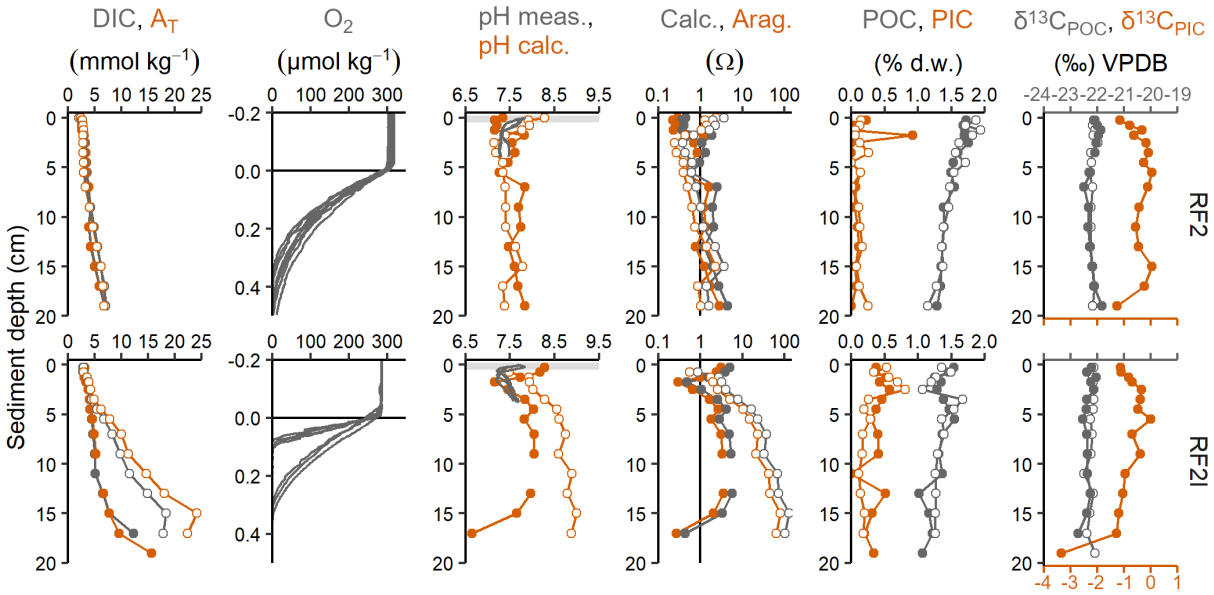

Figure 3 Porewater and solid phase profiles from stations RF2 and RF2I. Filled and empty markers represent replicate sediment cores, grey lines represent microprofiling data. The light grey area in the pH graph marks the scale of the O_2 graph. Note the differences in scales on both x and y axes between plots.

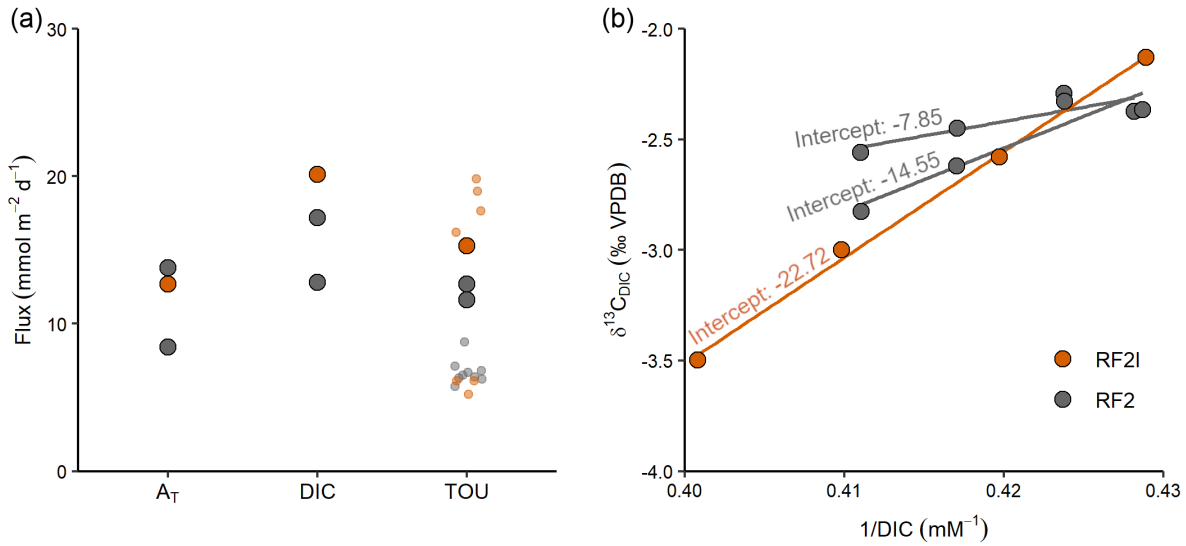

Figure 4 **(a)** Sediment-water fluxes of alkalinity (A_T), dissolved inorganic carbon (DIC), and total oxygen uptake (TOU) from RF2 (grey) and RF2I (orange). Large circles mark fluxes measured in the incubation chambers; small circles mark diffusive O_2 uptake rates from microprofiling data. **(b)** Keeling plot showing the DIC concentration and $\delta^{13}C$ composition ($\delta^{13}C_{DIC}$) in the incubations. The calculated intercepts indicate the $\delta^{13}C$ signal of the combined DIC sources in each incubation.

uptake (TOU) measured in the chamber was 15 mmol m^{-2} d^{-1}. At RF2, the diffusive O_2 uptake was 6–9 mmol m^{-2} d^{-1}, and the TOU was 11–12 mmol m^{-2} d^{-1}. Small scale differences in sediment-water solute exchange, as indicated by microprofiles, suggest heterogeneous chemical conditions within the sediment at RF2I, whereas the TOU over the larger surface area of the incubation chamber approached that at RF2.

Carbonate Dynamics and Ikaite Formation

Analysis by XRD confirmed the mineral as ikaite (a = 8.760 Å, b = 8.305 Å, c = 11.000 Å, β = 110.477, space group C2/c). The ikaite $\delta^{13}C$ values (−49.8 to −53.8 ‰), the lowest reported for ikaite and glendonite (Fig. 2c; Rogov *et al.*, 2020, 2021), indicate carbon derived from DIC formed during AOM (Greinert and Derkachev, 2004; Hiruta and Matsumoto, 2022). At site RF2I, very high porewater saturation states for aragonite (>80) and calcite (>100; Fig. 3) suggest that the precipitation of these phases was suppressed, allowing A_T to accumulate to levels conducive for ikaite formation. Porewater concentrations of phosphorus, Mg and sulfur, known inhibitors of calcite and aragonite growth (Bischoff *et al.*, 1993; Tollefsen *et al.*, 2018), were within expected ranges for coastal sediments at RF2 (Schulz, 2006; Ruttenberg, 2014; Fig. S-3). Assuming the main difference between sites was the upward migration of CH_4-rich porewater at RF2I, these results indicate that aragonite and

calcite precipitation can be suppressed under typical coastal conditions, enabling ikaite formation at cold temperatures and a high A_T supply.

The $\delta^{13}C_{PIC}$ at RF2 and RF2I (Fig. 3), along with decreasing porewater Ca and Mg with depth at RF2 (Fig. S-3), indicate authigenic carbonate precipitation within the top 20 cm of sediment. Increasingly negative $\delta^{13}C_{PIC}$ values with depth suggest *in situ* PIC formation incorporating isotopically light DIC from organic matter mineralisation or AOM (Campbell, 2006). More negative $\delta^{13}C_{PIC}$ values at RF2I (−3.35 to 0.00 ‰) compared to RF2 (−1.2 to 0.05 ‰) imply more intense carbonate formation or a greater contribution of AOM derived DIC. Contrasting carbonate dynamics are also reflected in the $\delta^{13}C$ composition of the sediment-water DIC flux, with lighter DIC released at RF2I (Fig. 4b). Assuming organic matter degradation and carbonate dissolution are the only DIC sources, their relative contributions were estimated from a Keeling plot (Pataki *et al.*, 2003). Carbonate dissolution contributed 36–66 % of the DIC efflux at RF2 (SI), consistent with aragonite and calcite undersaturation in the top 5–10 cm of sediment (Fig. 3). At RF2I, the Keeling plot indicated no dissolution, although isotopically light DIC from CH_4 oxidation was not considered and may have obscured any dissolution signal.

Ikaite as an Indicator of Methane

This study reports the discovery of ikaite near the sediment surface (<40 cm) in an Icelandic fjord. While our data suggest formation driven by AOM, alternative mechanisms should be considered. Volcanic ash diagenesis can enhance carbonate saturation and promote ikaite precipitation (Vickers *et al.*, 2024), but this is unlikely here given the absence of nearby volcanic activity (Thordarson and Höskuldsson, 2008) and the mineralogical similarities between RF2 and RF2I (Fig. S-2). Ikaite formation can also occur *via* seepage of highly alkaline groundwater, as observed in the Ikka fjord (Buchardt *et al.*, 1997). The proximity to the Helgustaðir mine, where Icelandic spar was historically extracted, and faults in the region (Karson *et al.*, 2018), indicate that such inputs are possible. However, the exceptionally low $\delta^{13}C_{ikaite}$ values strongly suggest mineral formation driven by intense AOM fuelled by a deep CH_4 source; a hypothesis supported by porewater geochemistry and sub-bottom profiling indicating the presence of gas below the site.

Accordingly, ikaite provides indirect evidence that CH_4 reaches the surface sediment at some locations in the investigated fjord. Although reports of CH_4 in coastal Icelandic sediments are rare, both biogenic and thermogenic sources have been identified at CH_4 seeps in northern Iceland (Þorsteinsdóttir *et al.*, 2020). The CH_4 origin here cannot be resolved from the $\delta^{13}C_{ikaite}$ as multiple DIC sources influenced the porewater $\delta^{13}C_{DIC}$ (Teichert and Luppold, 2013), but the light isotopic signal may indicate a biogenic source (Whiticar, 1999). This interpretation is further supported by the lack of volcanic activity in the area and $\delta^{13}C_{ikaite}$ values lower than those associated with thermogenically formed CH_4 in hydrothermal fluids in Iceland (Stefánsson *et al.*, 2024).

The sediment accumulation rate measured by ^{210}Pb at RF2 was 0.43 cm yr^{-1} (SI). Assuming the same accumulation rate at RF2I, the ikaite would be no more than 93 years old if it were the same age as the surrounding sediment. It is plausible that the crystals were considerably younger, since the ikaite likely was not formed at the sediment-water interface but deeper in the sediment where carbonate supersaturation was reached (Lu *et al.*, 2012; Whiticar *et al.*, 2022). There is no evidence of substantial CH_4 emissions from the sediment, such as pockmarks, suggesting that the occurrence of ikaite was very localised. Yet, the presence of CH_4 derived ikaite so close to the sediment surface substantially expands the environmental range within which the mineral is known to form, and confirms the usability of ikaite and glendonite $\delta^{13}C$ to track CH_4 seeps in cold water environments.

Acknowledgments

The authors thank the captain and crew of the RV *Belgica* for assistance at sea, Yannick Stroobandt at KU Leuven for carbon isotope analysis, Daniel Borschneck at CEREGE for assistance with the powder XRD analysis, and Dimitris Triandafillidis at HARBOR for assistance with single crystal XRD data collection. This research was supported by the Belgian Federal Science Policy Office (grant no RV/21/DEHEAT). AH was funded by a junior postdoctoral fellowship from Research Foundation – Flanders (FWO; grant no. 1241724N) and a Marie Sklodowska-Curie Individual Fellowship (MSCA; grant no. 101204337). SA was funded by the F.R.S.-FNRS (FIESTA, grant no. 35266740). JPB was funded by the US National Science Foundation (OCE-2241721) and the Lehigh CAS Dean's Opportunity Grant. KH was funded by Queens' College, University of Cambridge, and the Natural Environment Research Council (SiCLING, grant no. NE/X014819/1). RKJ was funded by MSCA (grant no. 101060342). PL, LV, and CW were funded by PhD fellowships from FWO (grants no. 1139224N, 1114521N, and 11P8Z24N). We thank Bo Schultz and an anonymous reviewer for constructive comments on the manuscript.

Editor: Gavin Foster

Additional Information

Supplementary Information accompanies this letter at https://www.geochemicalperspectivesletters.org/article2621.

Cite this letter as: Hylén, A., Arndt, S., Balmonte, J.P., Bosman, R., Bui, W., Chou, L., Delbono, I., Goossens, C., Hall, P.O.J., Hidalgo-Martinez, S., James, R.K., Kononets, M., Ley, P., März, C., Purayil, S.P., Reardon, J., Reyniers, P., Sales de Freitas, F., Verweirder, L., Wagner, K., Wittig, C., Hendry, K.R., van de Velde, S.J. (2026) Ikaite precipitation indicates near surface occurrence of methane in an Icelandic fjord. *Geochem. Persp. Let.* 40, 43–48. https://doi.org/10.7185/geochemlet.2621

References

Berner, R.A. (1970) Sedimentary pyrite formation. *American Journal of Science* 268, 1–23. https://doi.org/10.2475/ajs.268.1.1

Bischoff, J.L., Fitzpatrick, J.A., Rosenbauer, R.J. (1993) The Solubility and Stabilization of Ikaite ($CaCO_3{\cdot}6H_2O$) from 0° to 25°C: Environmental and Paleoclimatic Implications for Thinolite Tufa. *The Journal of Geology* 101, 21–33. https://doi.org/10.1086/648194

Buchardt, B., Seaman, P., Stockmann, G., Vous, M., Wilken, U., Düwel, L., Kristiansen, A., Jenner, C., Whiticar, M.J., Kristensen, R.M., Petersen, G.H., Thorbjørn, L. (1997) Submarine columns of ikaite tufa. *Nature* 390, 129–130. https://doi.org/10.1038/36474

Campbell, K.A. (2006) Hydrocarbon seep and hydrothermal vent paleoenvironments and paleontology: Past developments and future research directions. *Palaeogeography, Palaeoclimatology, Palaeoecology* 232, 362–407. https://doi.org/10.1016/j.palaeo.2005.06.018

Egger, M., Riedinger, N., Mogollón, J.M., Jørgensen, B.B. (2018) Global diffusive fluxes of methane in marine sediments. *Nature Geoscience* 11, 421–425. https://doi.org/10.1038/s41561-018-0122-8

EMODnet Bathymetry Consortium (2024) https://doi.org/10.12770/cf51df64-56f9-4a99-b1aa-36b8d7b743a1

Greinert, J., Derkachev, A. (2004) Glendonites and methane-derived Mg-calcites in the Sea of Okhotsk, Eastern Siberia: implications of a venting-related ikaite/glendonite formation. *Marine Geology* 204, 129–144. https://doi.org/10.1016/S0025-3227(03)00354-2

Hiruta, A., Matsumoto, R. (2022) Geochemical comparison of ikaite and methane-derived authigenic carbonates recovered from Echigo Bank in the Sea of Japan. *Marine Geology* 443, 106672. https://doi.org/10.1016/j.margeo.2021.106672

James, R.H., Bousquet, P., Bussmann, I., Haeckel, M., Kipfer, R., Leifer, I., Niemann, H., Ostrovsky, I., Piskozub, J., Rehder, G., Treude, T., Vielstädte, L., Greinert, J. (2016) Effects of climate change on methane emissions from seafloor sediments in the Arctic Ocean: A review. *Limnology and Oceanography* 61, S283–S299. https://doi.org/10.1002/lno.10307

Judd, A.G., Hovland, M. (1992) The evidence of shallow gas in marine sediments. *Continental Shelf Research* 12, 1081–1095. https://doi.org/10.1016/0278-4343(92)90070-Z

Karson, J.A., Farrell, J.A., Chutas, L.A., Nanfito, A.F., Proett, J.A., Runnals, K.T., Sæmundsson, K. (2018) Rift-Parallel Strike-Slip Faulting Near the Iceland Plate Boundary Zone: Implications for Propagating Rifts. *Tectonics* 37, 4567–4594. https://doi.org/10.1029/2018TC005206

Kennedy, G.L. (2022) Glendonites: Enigmatic Mineral Pseudomorphs and Their Ephemeral Precursor. *Rocks and Minerals* 97, 496–509. https://doi.org/10.1080/00357529.2022.2087146

Kolesnik, O.N., Kolesnik, A.N., Karabtsov, A.A., Vasilenko, Yu. P., Gorbarev, A.A. (2025) Ikaite from Holocene Sediments of the Chukchi Sea. *Doklady Earth Sciences* 520, 3. https://doi.org/10.1134/S1028334X24604383

Lu, Z., Rickaby, R.E.M., Kennedy, H., Kennedy, P., Pancost, R.D., Shaw, S., Lennie, A., Wellner, J., Anderson, J.B. (2012) An ikaite record of late Holocene climate at the Antarctic Peninsula. *Earth and Planetary Science Letters* 325–326, 108–115. https://doi.org/10.1016/j.epsl.2012.01.036

Morales, C., Rogov, M., Wierzbowski, H., Ershova, V., Suan, G., Adatte, T., Föllmi, K.B., Tegelaar, E., Reichart, G.-J., de Lange, G.J., Middelburg, J.J., van de Schootbrugge, B. (2017) Glendonites track methane seepage in Mesozoic polar seas. *Geology* 45, 503–506. https://doi.org/10.1130/G38967.1

Pataki, D.E., Ehleringer, J.R., Flanagan, L.B., Yakir, D., Bowling, D.R., Still, C.J., Buchmann, N., Kaplan, J.O., Berry, J.A. (2003) The application and interpretation of Keeling plots in terrestrial carbon cycle research. *Global Biogeochemical Cycles* 17. https://doi.org/10.1029/2001GB001850

Pauly, H. (1963) "Ikaite", a new mineral from Greenland. *Arctic* 16, 263–264. https://doi.org/10.14430/arctic3545

Rogov, M., Ershova, V., Vereshchagin, O., Vasileva, K., Mikhailova, K., Krylov, A. (2021) Database of global glendonite and ikaite records throughout the Phanerozoic. *Earth System Science Data*. Copernicus GmbH 13, 343–356. https://doi.org/10.5194/essd-13-343-2021

Rogov, M., Vasileva, K., Mikhailova, K., Ershova, V. (2020) Database of global glendonite and ikaite records throughout the Phanerozoic. *Zenodo*. https://doi.org/10.5281/ZENODO.7833894

Ruttenberg, K.C. (2014) The Global Phosphorus Cycle. In: Holland, H.D., Turekian, K.K. (Eds.) *Treatise on Geochemistry (Second Edition)*. Elsevier, Oxford, 499–558. https://doi.org/10.1016/B978-0-08-095975-7.00813-5

Schubert, C.J., Nürnberg, D., Scheele, N., Pauer, F., Kriews, M. (1997) ^{13}C isotope depletion in ikaite crystals: evidence for methane release from the Siberian shelves? *Geo-Marine Letters* 17, 169–174. https://doi.org/10.1007/s003670050023

Schultz, B., Thibault, N., Huggett, J. (2022) The minerals ikaite and its pseudomorph glendonite: Historical perspective and legacies of Douglas Shearman and Alec K. Smith. *Proceedings of the Geologists' Association* 133, 176–192. https://doi.org/10.1016/j.pgeola.2022.02.003

Schulz, H.D. (2006) Quantification of Early Diagenesis: Dissolved Constituents in Pore Water and Signals in the Solid Phase. In: Schulz, H.D., Zabel, M. (Eds.) *Marine Geochemistry*. Springer-Verlag, Berlin/Heidelberg, 73–124. https://doi.org/10.1007/3-540-32144-6_3

Stefánsson, A., Ricci, A., Garnett, M., Gunnarsson-Robin, J., Kleine-Marshall, B.I., Scott, S.W., Lelli, M., Cardoso, C.D., Pik, R., Santinelli, C., Ono, S., Barry, P.H., Broadley, M.W., Byrne, D., Halldórsson, S.A., Fiebig, J. (2024) Isotopic and kinetic constraints on methane origins in Icelandic hydrothermal fluids. *Geochimica et Cosmochimica Acta* 373, 84–97. https://doi.org/10.1016/j.gca.2024.03.015

Teichert, B.M.A., Luppold, F.W. (2013) Glendonites from an Early Jurassic methane seep — Climate or methane indicators? *Palaeogeography, Palaeoclimatology, Palaeoecology* 390, 81–93. https://doi.org/10.1016/j.palaeo.2013.03.001

Thordarson, T., Höskuldsson, Á. (2008) Postglacial volcanism in Iceland. *Jökull* 58, 197–228. https://doi.org/10.33799/jokull2008.58.197

Tollefsen, E., Stockmann, G., Skelton, A., Mörth, C.-M., Dupraz, C., Sturkell, E. (2018) Chemical controls on ikaite formation. *Mineralogical Magazine* 82, 1119–1129. https://doi.org/10.1180/mgm.2018.110

Vickers, M.L., Jones, M.T., Longman, J., Evans, D., Ullmann, C.V., Wulfsberg Stokke, E., Vickers, M., Frieling, J., Harper, D.T., Clementi, V.J., IODP Expedition 396 Scientists (2024) Paleocene–Eocene age glendonites from the Mid-Norwegian Margin – indicators of cold snaps in the hothouse? *Climate of the Past* 20, 1–23. https://doi.org/10.5194/cp-20-1-2024

Vickers, M.L., Vickers, M., Rickaby, R.E.M., Wu, H., Bernasconi, S.M., Ullmann, C.V., Bohrmann, G., Spielhagen, R.F., Kassens, H., Pagh Schultz, B., Alwmark, C., Thibault, N., Korte, C. (2022) The ikaite to calcite transformation: Implications for palaeoclimate studies. *Geochimica et Cosmochimica Acta* 334, 201–216. https://doi.org/10.1016/j.gca.2022.08.001

Whiticar, M.J. (1999) Carbon and hydrogen isotope systematics of bacterial formation and oxidation of methane. *Chemical Geology* 161, 291–314. https://doi.org/10.1016/S0009-2541(99)00092-3

Whiticar, M.J., Suess, E., Wefer, G., Müller, P.J. (2022) Calcium Carbonate Hexahydrate (Ikaite): History of Mineral Formation as Recorded by Stable Isotopes. *Minerals* 12, 1627. https://doi.org/10.3390/min12121627

Zhou, X., Lu, Z., Rickaby, R.E.M., Domack, E.W., Wellner, J.S., Kennedy, H.A. (2015) Ikaite Abundance Controlled by Porewater Phosphorus Level: Potential Links to Dust and Productivity. *The Journal of Geology* 123, 269–281. https://doi.org/10.1086/681918

Porsteinsdóttir, G.V., Blischke, A., Sigurbjörnsdóttir, M.A., Òskarsson, F., Arnarson, P.S., Magnússon, K.P., Vilhelmsson, O. (2020) Gas seepage pockmark microbiomes suggest the presence of sedimentary coal seams in the Öxarfjörður graben of northeastern Iceland. *Canadian Journal of Microbiology* 66, 25–38. https://doi.org/10.1139/cjm-2019-0081

Geochemical Perspectives Letters

Ikaite precipitation indicates near-surface occurrence of methane in an Icelandic fjord

A. Hylén[1,2], S. Arndt[3,4], J.P. Balmonte[5], R. Bosman[6], W. Bui[3], L. Chou[3], I. Delbono[7], C. Goossens[1], P.O.J. Hall[8], S. Hidalgo-Martinez[1], R.K. James[3,9], M. Kononets[8,10], P. Ley[1], C. März[11], S.P. Purayil[12], J. Reardon[13], P. Reyniers[14], F. Sales de Freitas[3], L. Verweirder[14], K. Wagner[11], C. Wittig[15], K.R. Hendry[16,17], S.J. van de Velde[1,18,19]

[1]Geobiology Research Group, Department of Biology, University of Antwerp, Universiteitsplein 1, 2610 Wilrijk, Belgium
[2]Aix-Marseille Université, CNRS, IRD, INRAE, CEREGE, Technopôle de l'Arbois-Méditerranée, BP80, 13545 Aix-en-Provence, France
[3]BGeoSys, Department Geosciences, Society and Environment, Université Libre the Bruxelles, Brussels, Belgium
[4]iC3, Department of Geoscience, Arctic University of Norway, Tromso, Norway
[5]Department of Earth and Environmental Sciences, Lehigh University, USA
[6]Institute for Biochemistry and Signal Transduction, University Medical Center Hamburg-Eppendorf, Martinistraße 52, 20246 Hamburg, Germany
[7]ENEA Marine Environment Research Centre, Department for Sustainability, Laboratory of Biodiversity and Ecosystems, 19032 Pozzuolo di Lerici (La Spezia), Italy
[8]Department of Marine Sciences, University of Gothenburg, Box 461, 405 30 Gothenburg, Sweden
[9]Department of Biology, University of Southern Denmark, Odense Denmark
[10]Research consultant, Fredrikas Gård 2, 414 83, Gothenburg, Sweden
[11]Institute for Geosciences, University of Bonn, Kirschallee 1-3, 53115 Bonn, Germany
[12]Operational Directorate Natural Environment, Royal Belgian Institute of Natural Sciences, Brussels, Belgium
[13]External Relations Team, University of Southern Denmark, Odense, Denmark
[14]Department of Geology, Ghent University, Krijgslaan 297, 9000 Ghent, Belgium
[15]Marine Biology Research Group, Ghent University, Ghent, Belgium
[16]British Antarctic Survey, High Cross, Madingley Road, Cambridge, CB3 0ET, UK
[17]Queens' College, University of Cambridge, Silver Street, Cambridge, CB3 9ET, UK
[18]Department of Marine Science, University of Otago, Ōtepoti Dunedin, 9016, Aotearoa New Zealand
[19]Earth Sciences New Zealand, Te Whanganui-a-Tara Wellington, 6021, Aotearoa New Zealand

Supplementary Information

The Supplementary Information includes:

- Methods
- Table S-1
- Figures S-1 to S-3
- Supplementary Information References

The data described in this publication is available in an accompanying dataset (Hylén *et al.,* 2026).

Bottom water conditions and seafloor mapping

Prior to sediment sampling, a CTD (SBE9plus, Sea-Bird Scientific) equipped with an oxygen (O_2) sensor (SBE43, Sea-Bird Scientific) was deployed to record the bottom-water conditions. The bottom water had a salinity of 34.4, a temperature of 4.2 °C, and the O_2 concentration was 287 µmol kg^{-1}.

The hull-mounted Kongsberg EM2040 Dual RX multibeam echosounder onboard RV Belgica was used to acquire bathymetric data. The data were processed using QPS Qimera v2.5.3. This involved time–depth conversion using sound velocity profiles derived from the CTD measurements gathered during the survey, manual noise removal, and gridding the bathymetry at a 5 m resolution.

Sub-bottom data were acquired using a hull-mounted TOPAS PS18 Parametric Sub-Bottom Profiler system operating with a Ricker pulse at 6 kHz. The data were processed in RadExPro v2022.4 using deconvolution, a Butterworth bandpass filter, and amplitude correction. The processed profile has a vertical resolution of about 0.2 m and a maximum penetration depth of about 50 ms two-way travel time. Sub-bottom depths were calculated using a constant sound velocity of 1470 m s^{-1}, which is based on temperature and salinity measurements of the bottom waters at station RF2.

Sediment-water flux incubations

Sediment for sediment-water flux incubations was collected with a NIOZ-type box corer (Ø 50 cm). Three replicate cores were collected approximately 5 m apart and the depth of the collected sediment was approximately 40 cm. The top ~20 cm of sediment in each box core was subsequently sub-cored with a cylindrical incubation chamber (Ø 14.4 cm), which was closed with a gas-tight lid. The cores were then incubated for 19 hours. Concentrations of O_2 were measured continuously using probes (Firesting), and the O_2 fluxes were calculated from the best-fitting slope of concentration versus time over the whole incubation ($R^2 > 0.99$ on average for the incubations). At five time points, discrete water samples of 12 mL and 6 mL

were collected in Exetainers (Labco) for analysis of DIC concentrations and isotopic composition ($\delta^{13}C_{DIC}$), respectively. The DIC samples were analysed within 24 hours, while the $\delta^{13}C_{DIC}$ samples were preserved with 20 µL saturated $HgCl_2$ for later analysis (see below). At the first and last time points, water samples of 50 mL were filtered (0.45 µm, PES) into centrifuge tubes (Falcon) for analysis of alkalinity (A_T) onboard within a few days (see below). The concentrations of A_T and DIC were corrected for dilution during sampling before calculation of the sediment-water fluxes using FLUXER (Hylén and van de Velde, 2025).

Sediment and porewater sampling

Two replicate sediment cores for geochemical profiling were collected with a GEMAX corer (Ø 9 cm) at RF2, or were subcored (Ø 5.9 cm) from the ikaite-site incubation chamber at RF2I. Prior to sediment slicing, the cores were used for microsensor profiling (see below). The cores were sliced at a 0.5-2 cm resolution for determination of solid phase carbon and porewater DIC and A_T. Samples were transferred to centrifuge tubes and were centrifuged at 2800 g for 10 minutes, after which the supernatant was filtered (0.45 µm, PES) into 3 mL Exetainers, which were capped without headspace before storage at 6 °C until analysis within 24 h. The remaining solid phase was freeze-dried and ground in an agate mortar for analysis of carbon and mineralogy.

At station RF2, three more GEMAX cores were collected. Two of the cores were subcored (Ø 5.9 cm) and were sliced under an N_2 atmosphere (Captair Field pyramid, Erlab) at the same resolution as above. The sediment was transferred to centrifuge tubes and Rhizons samplers (MOM; Rhizosphere) were inserted into the sediment to extract porewater for elemental analysis. The porewater was acidified with 15 µL concentrated HNO_3 per mL sample. The remaining solid phase was freeze-dried and stored in aluminum bags under N_2 atmosphere for iron (Fe) and sulfur (S) speciation. The third core was sliced at the same resolution above and was freeze-dried for the determination of porosity and sediment accumulation rates.

Ikaite crystals found at RF2I were immediately frozen. Before further processing, the crystals were rinsed with cold (<2 °C) deionized water.

Microsensor profiling

At station RF2, two replicate sediment cores collected with a GEMAX corer (Ø 9 cm) were subcored (Ø 5.9 cm, 20 cm sediment, ca. 5 cm overlaying water). At station RF2I, two replicate subcores (Ø 4.0 cm, 10 cm sediment) were collected from the sediment used for flux incubations. The latter cores were submerged in bottom water from RF2I in an aquarium. The overlying water of both core types was continuously aerated using an aquarium pump. Microsensor profiling of O_2 (50 µm tip), hydrogen sulfide (H_2S; 100 µm tip) and

pH (200 µm tip) was performed using commercially available microsensors, a multimeter amplifier and a motorized micromanipulator (Unisense A.S., Denmark). Microsensors were calibrated as described previously (Malkin *et al.*, 2014).

Diffusive O_2 fluxes (J_{O2}) were calculated according to Fick's first law from the O_2 porewater profiles:

$$J_{O2} = -\frac{\varphi D_0}{\theta^2} \cdot \frac{\partial C_{O2}}{\partial z} \quad \text{Eq. S-1}$$

where φ is the porosity, D_0 is the molecular diffusion coefficient for O_2 in water, θ is the tortuosity and $\partial C_{O2}/\partial z$ is the linear part of the slope of the O_2 concentration profile over depth. The value of D_0 was calculated as a function of the temperature and salinity using the R package *marelac* (Soetaert *et al.*, 2020), and θ was calculated through the modified Weissberg relation (Boudreau, 1996):

$$\theta^2 = 1 - 2\ln(\varphi) \quad \text{Eq. S-2}$$

Analysis of porewater and incubation water

Concentrations of DIC were determined on board the ship by non-dispersive infrared determination of CO_2 gas (LI-6262/LI-850, LI-COR) after acidification with phosphoric acid. Incubation water samples were analyzed on an Apollo C5L (Apollo SciTech, USA), and porewater was measured using a custom-built DIC analyzer (Nilsson *et al.*, 2019). Repeated measurements of certified reference material (CRM; batch 189 from Dickson Laboratory, Scripps Inst. of Oceanography) were conducted to calibrate the instruments and correct for potential drift in the systems. Repeated measurements of certified reference material (CRM; batch 189 from Dickson Laboratory, Scripps Inst. of Oceanography) were conducted to calibrate the instruments and correct for potential drift in the systems. The analytical precision was 0.2 % relative standard deviation (RSD) for the flux samples and better than 0.6 % RSD for the porewater samples.

The $\delta^{13}C_{DIC}$ values of the samples from the flux incubations were measured on a GasBench II coupled to an isotope ratio mass spectrometer (IRMS; Thermo Delta Plus XP, Thermo Fisher Scientific), and were corrected for isotope fractionation between dissolved and gaseous CO_2. Data were calibrated using the CRMs LSVEC and NBS19 and in-house standards Merck ($\delta^{13}C$ = -9.65 ‰) and Fluka ($\delta^{13}C$ = 2.36 ‰). The precision was <0.08 ‰ (standard deviation; SD) and results are expressed relative to VPDB.

Samples for A_T were analyzed by open-cell potentiometric titration using an automated titrator setup (888 Titrando, Metrohm) according to Dickson *et al.* (2007). The titrator was calibrated using the same CRM as for the DIC concentration analysis and an internal standard (ultrafiltered seawater, 2404 ± 8 µM A_T) was run alongside the samples. The analytical precision was 0.3 % RSD. Due to low volumes (~2 mL), porewater A_T samples were diluted with ultrafiltered seawater to a final volume of 50 mL before analysis. Major and minor

elements in the porewater were measured on an inductive coupled plasma – optical emission spectrometer (ICP-OES; iCAP PRO X Duo, Thermo Fisher). Beryllium and Yttrium were used as internal standards (informative). CRMs CASS-6 and SLEW-4 were spiked and used for quality control. The precision was generally <1 % RSD for most elements and < 3 % for P and Li.

Solid phase carbon analysis

The sedimentary total carbon (TC) concentration and stable isotope carbon composition ($\delta^{13}C_{TC}$) were measured on an elemental analyzer (EA; EA 1110, CE Instruments) connected via a Conflo IV interface (Thermo Fisher Scientific) to an IRMS (Thermo Delta V Advantage, Thermo Fisher Scientific). Data were calibrated using the CRM IAEA-600 and in-house standards leucine ($\delta^{13}C$ = -13.73 ‰, carbon content = 54.72 %) and tuna ($\delta^{13}C$ = -17.96 ‰, carbon content = 45.24 %), calibrated against different CRMs. The precision was <2 % RSD for the carbon content and <0.08 ‰ SD for $\delta^{13}C$, and the $\delta^{13}C$ results are expressed relative to VPDB. The particulate organic carbon (POC) concentration and isotopic composition ($\delta^{13}C_{POC}$) were measured as described above after removal of inorganic carbon from the freeze-dried sediment after treatment with 0.5 M HCl. The sedimentary content of particulate inorganic carbon (PIC) was calculated by subtracting POC from TC. The isotopic compositions of PIC ($\delta^{13}C_{PIC}$) and parts of a freeze-dried ikaite crystal ($\delta^{13}C_{ikaite}$) were measured with the same method as the $\delta^{13}C_{DIC}$ samples.

Mineralogical determination by powder X-ray diffraction

Sediment samples were placed on low-background silicon plates, and mineralogy was identified using X-ray diffraction with an X'Pert Pro diffractometer (PANalytical) fitted with a cobalt tube (λ = 1.79 Å), operating at 40 kV and 40 mA. Samples were analysed from 5º (2θ) to 70º (2θ) with a step size of 0.026º, over a total duration of 2 hours and 7 minutes. The samples were spun at 15 rpm to improve statistics. Phase identification was performed using the software X'Pert HighScore Plus (PANalytical) together with the PDF-2 (Powder Diffraction File 2) database from the ICDD (International Center for Diffraction Data).

Solid phase iron and sulfur speciation

Particulate reactive Fe was extracted by treatment of freeze-dried sediment with 0.5 M HCl under agitation for 1 hour (Laufer *et al.*, 2020). The samples were centrifuged, and the concentrations of Fe(II) and Fe(III) in the supernatant were subsequently determined spectrophotometrically with the ferrozine method (Viollier *et al.*, 2000).

The sedimentary contents of acid reducible sulfides (AVS, e.g. FeS) and chromium reducible sulfides (CRS, e.g., FeS_2 and S_0) were determined through a two-step sequential extraction (Kallmeyer *et al.*, 2004). First, the AVS fraction was obtained by adding a 6 M HCl solution to freeze-dried sediment in a reaction flask. Over 40 minutes, the H_2S was stripped from the solution to a 5 % zinc acetate solution trap using N_2 as a carrier gas. The zinc acetate trap was subsequently replaced before addition of N,N di-methyl formamide (DMF) and a reduced chromium solution to the reaction flask for a further 40 minutes of extraction. The S in the traps was measured spectrophotometrically with the Cline method (Cline, 1969).

Porosity and sediment accumulation rates

The porosity of the sediment was determined from the weight loss after freeze drying, corrected for the salt content of the porewater. Radiometric analyses were performed by gamma spectrometry. Each sample was counted for 1-3 days on high-purity germanium detectors with carbon fiber windows for the detection of low-energy gamma rays. At a ^{60}Co gamma emission energy of 1.33 MeV, the detector efficiency was 60% with a resolution of 2.2 keV. Calibrations for ^{210}Pb and ^{226}Ra, ^{228}Th and ^{228}Ra were performed using an internal standard derived from the CANMET (Canadian Centre for Mineral and Energy Technology) reference standard DL1a and IAEA (International Atomic Energy Agency) reference standard RGTH1. The calibration for ^{137}Cs was performed using the multi-elemental reference standard QCYA48 from Eckert & Ziegler Analytics. Quality controls were routinely performed by analyzing the standard reference material IAEA-385. To evaluate the sediment accumulation rate (SAR), a numerical model that calculates radionuclide profiles in a sediment core affected by diffusion in a surficial layer was applied to the data (Buffoni *et al.*, 2020). The vertical profiles of ^{210}Pb excess, ^{137}Cs and ^{228}Th excess were simultaneously fitted to determine the best estimate of SAR.

Single-crystal X-ray diffraction

Frozen ikaite crystals were broken apart at 4 °C and attached to SPINE mounts and stored on ice. Samples were cryo-cooled under a N_2 cryostream (CryoJet XL, Oxford Instruments) set to 110 K. Manual alignment was performed along clearly discernible crystal edges to minimize overlapping lattices. Data collection was carried out on a XtaLAB Synergy-R diffractometer with a high-flux rotating anode (Rigaku). Data reduction was done in CrystalisPro and data was indexed and integrated into a = 8.760 Å, b = 8.305 Å, c = 11.000 Å, β = 110.477, space group C2/c, Rint = 0.099. The space group and unit cell contents were confirmed in ShelXT.

Calculation of contributions from different sources to the DIC flux

The contribution of carbonate dissolution to the DIC flux was calculated using the Keeling plot method (Keeling, 1958; Pataki *et al.*, 2003). The isotopic composition of the DIC being released from the sediment ($\delta^{13}C_{Sed}$) can be obtained by calculating the intercept of a regression of 1/DIC versus its $\delta^{13}C$ values ($\delta^{13}C_{DIC}$). We assume that DIC released from the sediment stems from either degradation of organic matter or dissolution of carbonates, so that:

$$1 = f_{POC} + f_{PIC} \quad \text{Eq. S-3}$$

where f_{POC} and f_{PIC} are the fractions of DIC produced through organic matter degradation and carbonate dissolution, respectively. Conservation of mass gives that:

$$\delta^{13}C_{Sed} = f_{POC} \cdot \delta^{13}C_{POC} + f_{PIC} \cdot \delta^{13}C_{PIC} \quad \text{Eq. S-4}$$

where $\delta^{13}C_{POC}$ and $\delta^{13}C_{PIC}$ are the average carbon isotope ratios of the solid phase organic and inorganic carbon, respectively, in the top 5 cm of sediment. The contribution from carbonate dissolution to the total DIC flux (f_{PIC}) can thereby be calculated by combining Eq. S-3 and Eq. S-4:

$$f_{PIC} = \frac{\delta^{13}C_{Sed} - \delta^{13}C_{POC}}{\delta^{13}C_{PIC} - \delta^{13}C_{POC}} \quad \text{Eq. S-5}$$

Data used for the calculations and the resulting f_{PIC} values are presented in Table S-1.

Supplementary Tables

Table S-1 Data used for calculating the contribution from carbonate dissolution to the sedimentary DIC flux (fPIC) and the resulting fPIC for each incubation chamber. The numbers for $\delta^{13}C_{POC}$ and $\delta^{13}C_{PIC}$ are average values for the top 5 cm of sediment at stations RF2 (chambers 1 and 3) and RF2I (chamber 2), and the uncertainty is the standard deviation of the measurements. The uncertainty for $\delta^{13}C_{Sed}$ is the standard error of the intercept on the Keeling plot.

Incubation chamber (station)	$\delta^{13}C_{Sed}$ (‰)	$\delta^{13}C_{POC}$ (‰)	$\delta^{13}C_{PIC}$ (‰)	f_{PIC}
1 (RF2)	-7.85 ± 2.32	-22.35 ± 0.08	-0.50 ± 0.26	0.66
3 (RF2)	-14.55 ± 2.91	-22.35 ± 0.08	-0.50 ± 0.26	0.36
2 (RF2I)	-22.72 ± 0.72	-22.22 ± 0.08	-0.71 ± 0.26	-0.02

Supplementary Figures

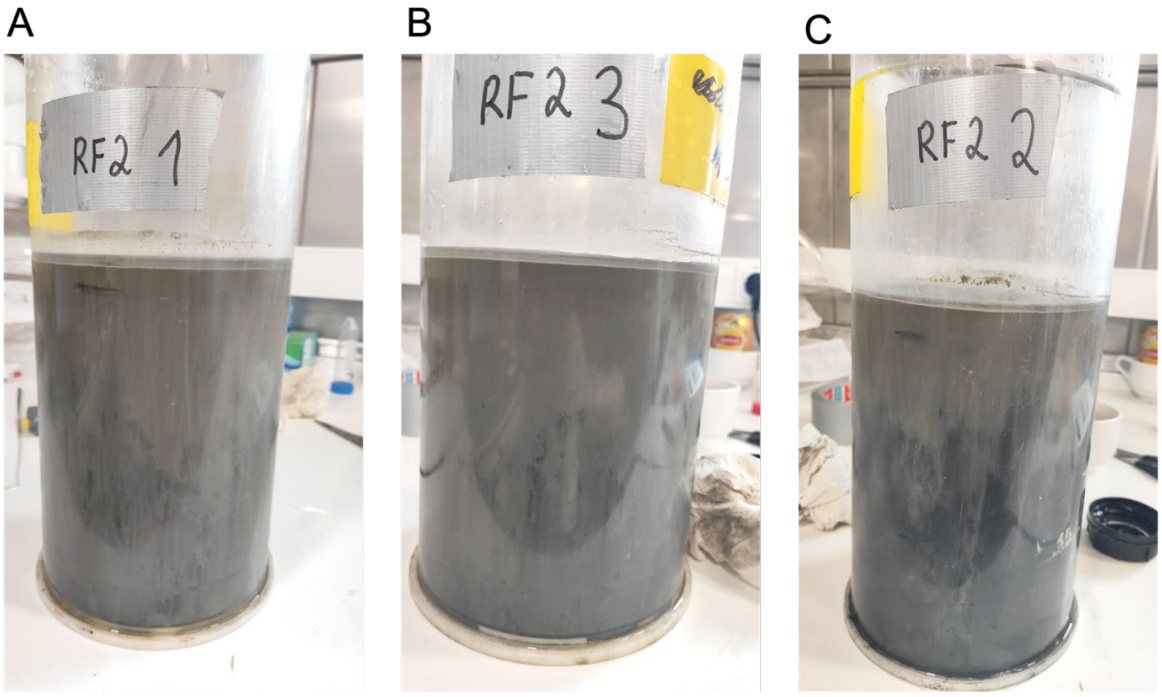

Figure S-1 Sediment after the end of the incubation. A and B show cores from RF2, C shows the core from RF2I.

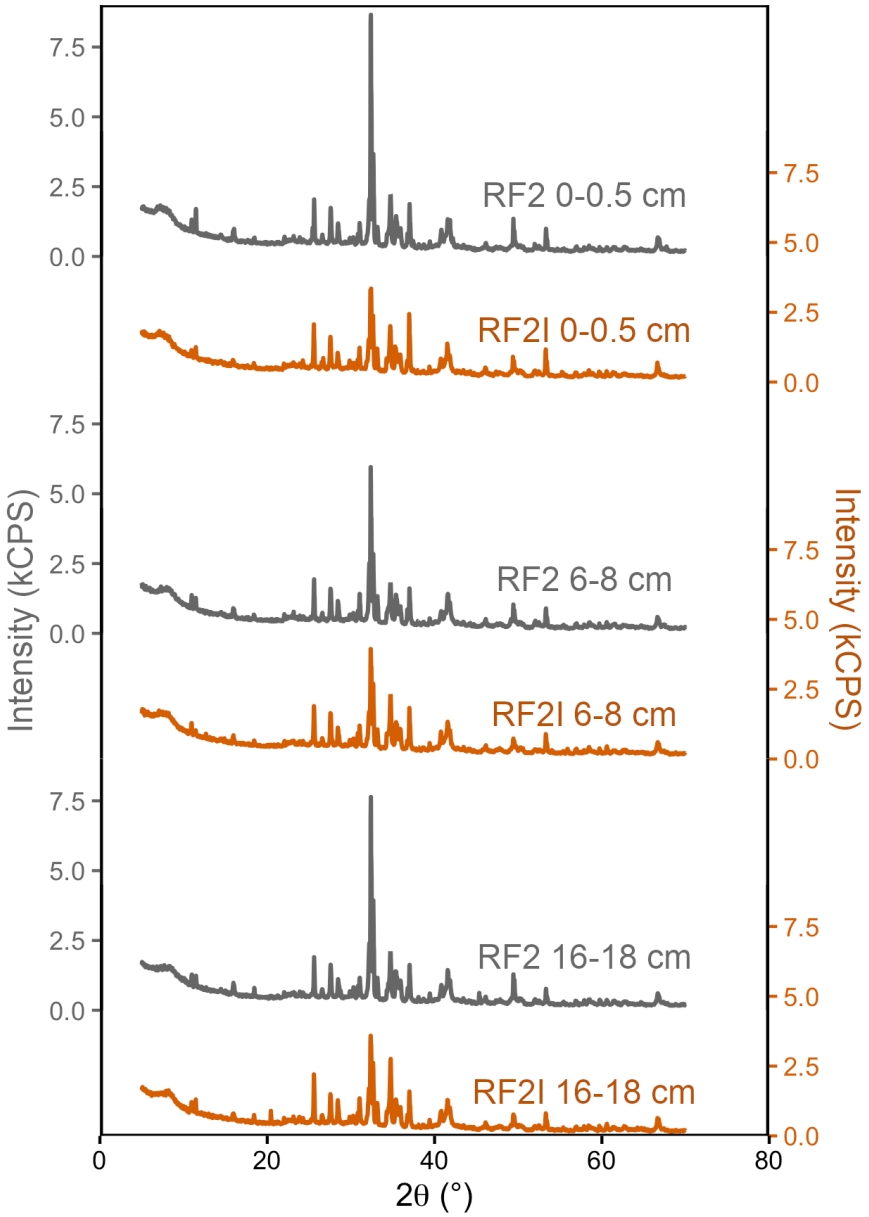

Figure S-2 XRD spectra from 0-0.5, 6-8, and 16-18 cm sediment depths at stations RF2 (grey) and RF2I (orange). The major phases identified were consistent across all samples and included andesine, diopside, chabazite, quartz, calcite, and halite (precipitated during sample drying). Note that the samples were handled and stored under oxic conditions, meaning oxygen-sensitive minerals may have been reoxidised.

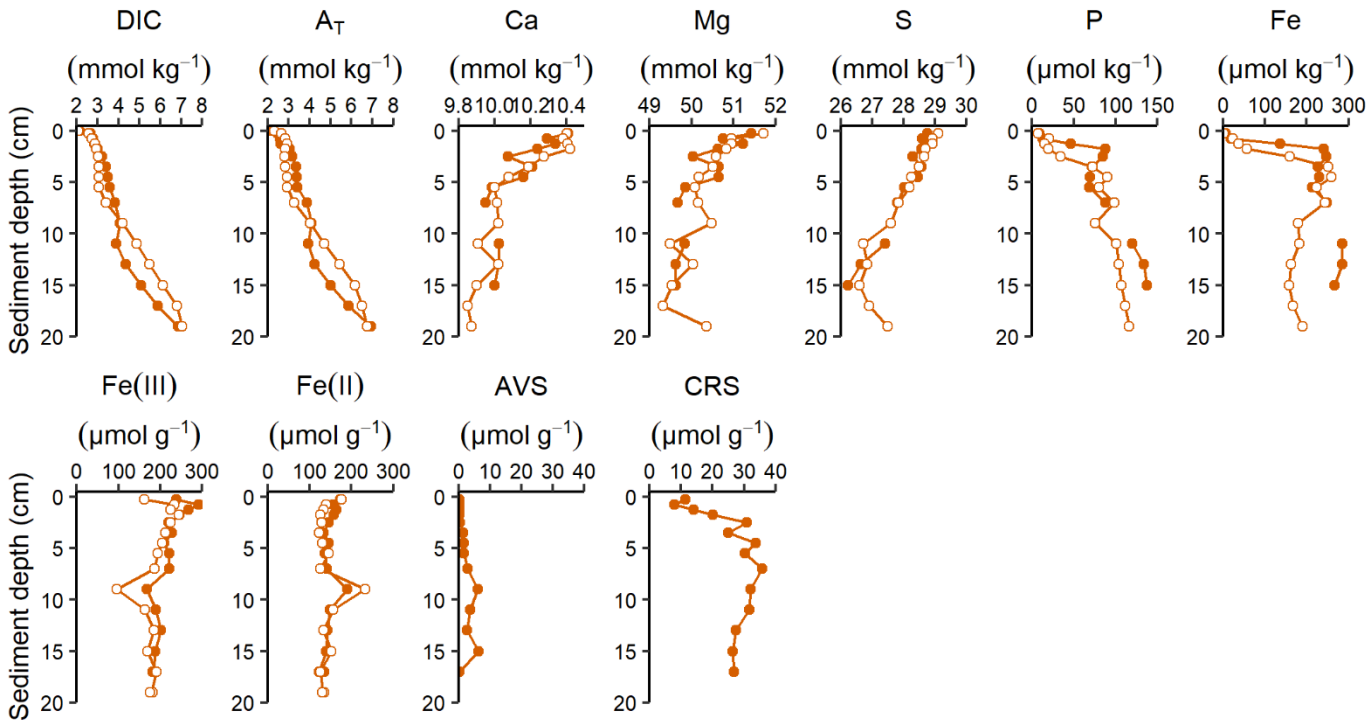

Figure S-3 Porewater profiles (top) and solid phase composition (bottom) at station RF2. Ca, Mg, S, P and Fe were measured by ICP-OES and are assumed to represent Ca^{2+}, Mg^{2+}, SO_4^{2-}, PO_4^{3-} and Fe^{2+}. Fe(III) = oxidized iron, Fe(II) = reduced iron, AVS = acid volatile sulphides, CRS = chromium reducible sulphides.

Supplementary Information References

Boudreau, B.P. (1996) The diffusive tortuosity of fine-grained unlithified sediments. *Geochimica et Cosmochimica Acta* 60, 3139–3142. https://doi.org/10.1016/0016-7037(96)00158-5

Buffoni, G., Schirone, A., Delfanti, R. (2020) A numerical investigation for dating 210Pbex and 137Cs vertical profiles in a coastal area: The Eastern Ligurian Sea, Italy. *Journal of Environmental Radioactivity* 212, 106122. https://doi.org/10.1016/j.jenvrad.2019.106122

Cline, J.D. (1969) Spectrophotometric determination of hydrogen sulfide. *Limnology and Oceanography* 14, 454–458. https://doi.org/10.4319/lo.1969.14.3.0454

Dickson, A.G., Sabine, C.L., Christian, J.R. (Eds.) (2007) *Guide to best practices for ocean CO_2 measurements*. PICES Special Publication 3, 191 pp.

Hylén, A., van de Velde, S. (2025) FLUXER. Zenodo. https://doi.org/10.5281/ZENODO.14758688

Hylén, A., Arndt, S., Balmonte, J.P., Bosman, R., Bui, W., Chou, L., Delbono, I., Goossens, C., Hall, P., Hidalgo Martinez, S., James, R.K., Kononets, M., Ley, P., März, C., Puthan Purayil, S., Reardon, J., Reyniers, P., Sales de Freitas, F., Verweirder, L., Wagner, K., Wittig, C., Hendry, K., van de Velde, S. (2026) Dataset for Ikaite precipitation indicates near-surface occurrence of methane in an Icelandic fjord. *Zenodo*. https://doi.org/10.5281/ZENODO.20053641

Kallmeyer, J., Ferdelman, T.G., Weber, A., Fossing, H., Jørgensen, B.B. (2004) A cold chromium distillation procedure for radiolabeled sulfide applied to sulfate reduction measurements. *Limnology and Oceanography: Methods* 2, 171–180. https://doi.org/10.4319/lom.2004.2.171

Keeling, C.D. (1958) The concentration and isotopic abundances of atmospheric carbon dioxide in rural areas. *Geochimica et Cosmochimica Acta* 13, 322–334. https://doi.org/10.1016/0016-7037(58)90033-4

Laufer, K., Michaud, A.B., Røy, H., Jørgensen, B.B. (2020) Reactivity of Iron Minerals in the Seabed Toward Microbial Reduction – A Comparison of Different Extraction Techniques. *Geomicrobiology Journal* 37, 170–189. https://doi.org/10.1080/01490451.2019.1679291

Malkin, S.Y., Rao, A.M., Seitaj, D., Vasquez-Cardenas, D., Zetsche, E.-M., Hidalgo-Martinez, S., Boschker, H.T., Meysman, F.J. (2014) Natural occurrence of microbial sulphur oxidation by long-range electron transport in the seafloor. *The ISME Journal* 8, 1843–1854. https://doi.org/10.1038/ismej.2014.41

Nilsson, M.M., Kononets, M.Y., Ekeroth, N., Viktorsson, L., Hylén, A., Sommer, S., Pfannkuche, O., Almroth-Rosell, E., Atamanchuk, D., Andersson, H.J., Roos, P., Tengberg, A., Hall, P.O.J. (2019) Organic carbon recycling in Baltic Sea sediments – An integrated estimate on the system scale based on in situ measurements. *Marine Chemistry* 209, 81–93. https://doi.org/10.1016/j.marchem.2018.11.004

Pataki, D.E., Ehleringer, J.R., Flanagan, L.B., Yakir, D., Bowling, D.R., Still, C.J., Buchmann, N., Kaplan, J.O., Berry, J.A. (2003) The application and interpretation of Keeling plots in terrestrial carbon cycle research. *Global Biogeochemical Cycles* 17. https://doi.org/10.1029/2001GB001850.

Soetaert, K., Petzoldt, T., Meysman, F.J.R., Meire, L. (2020) "marelac" R package, v. 2.1.10

Viollier, E., Inglett, P.W., Hunter, K., Roychoudhury, A.N., Van Cappellen, P. (2000) The ferrozine method revisited: Fe(II)/Fe(III) determination in natural waters. *Applied Geochemistry* 15, 785–790. https://doi.org/10.1016/S0883-2927(99)00097-9